

Published in final edited form as:

ACS Infect Dis. 2022 February 11; 8(2): 296–309. doi:10.1021/acscinfecdis.1c00432.

Development of Inhibitors of SAICAR Synthetase (PurC) from *Mycobacterium abscessus* Using a Fragment-Based Approach

Sitthivut Charoensutthivarakul,

Yusuf Hamied Department of Chemistry, University of Cambridge, Cambridge CB2 1EW, United Kingdom; School of Bioinnovation and Biobased Product Intelligence, Faculty of Science, Mahidol University, Bangkok 10400, Thailand

Sherine E. Thomas,

Department of Biochemistry, University of Cambridge, Cambridge CB2 1GA, United Kingdom

Amy Curran,

Yusuf Hamied Department of Chemistry, University of Cambridge, Cambridge CB2 1EW, United Kingdom

Karen P. Brown,

Molecular Immunity Unit, Department of Medicine, MRC Laboratory of Molecular Biology, University of Cambridge, Cambridge CB2 0QH, United Kingdom; Cambridge Centre for Lung Infection, Royal Papworth Hospital, Cambridge CB23 3RE, United Kingdom

Juan M. Belardinelli,

Mycobacteria Research Laboratories, Department of Microbiology, Immunology and Pathology, Colorado State University, Fort Collins, Colorado 80523-1682, United States

Andrew J. Whitehouse,

Yusuf Hamied Department of Chemistry, University of Cambridge, Cambridge CB2 1EW, United Kingdom

Marta Acebrón-García-de-Eulate,

Department of Biochemistry, University of Cambridge, Cambridge CB2 1GA, United Kingdom

Jaspar Sangan,

Molecular Immunity Unit, Department of Medicine, MRC Laboratory of Molecular Biology, University of Cambridge, Cambridge CB2 0QH, United Kingdom; Cambridge Centre for Lung Infection, Royal Papworth Hospital, Cambridge CB23 3RE, United Kingdom

Subramanian G. Gramani,

Corresponding Authors: **Anthony G. Coyne** - Yusuf Hamied Department of Chemistry, University of Cambridge, Cambridge CB2 1EW, United Kingdom; agc40@cam.ac.uk; **Tom L. Blundell** - Department of Biochemistry, University of Cambridge, Cambridge CB2 1GA, United Kingdom; tlb20@cam.ac.uk.

Author Contributions

C.A., A.G.C., T.L.B., R.A.F., V.M., and M.J. designed and supervised the project. S.C., A.C., A.J.W., and S.G.G. synthesized the compounds used in this study. S.E.T. and M.A.G.d.E. carried out the structural biology and biochemical studies. K.B. and J.S. devised and carried out the screening of the compounds against *Mab* and *Mtb*. J.M.B. and M.J. generated the knockout mutants. S.C., S.E.T., and A.G.C. wrote the manuscript, and all authors commented on the final version of the manuscript.

Notes

The authors declare no competing financial interest.

Yusuf Hamied Department of Chemistry, University of Cambridge, Cambridge CB2 1EW, United Kingdom

Mary Jackson,

Mycobacteria Research Laboratories, Department of Microbiology, Immunology and Pathology, Colorado State University, Fort Collins, Colorado 80523-1682, United States

Vitor Mendes,

Department of Biochemistry, University of Cambridge, Cambridge CB2 1GA, United Kingdom

R. Andres Floto,

Molecular Immunity Unit, Department of Medicine, MRC Laboratory of Molecular Biology, University of Cambridge, Cambridge CB2 0QH, United Kingdom; Cambridge Centre for Lung Infection, Royal Papworth Hospital, Cambridge CB23 3RE, United Kingdom

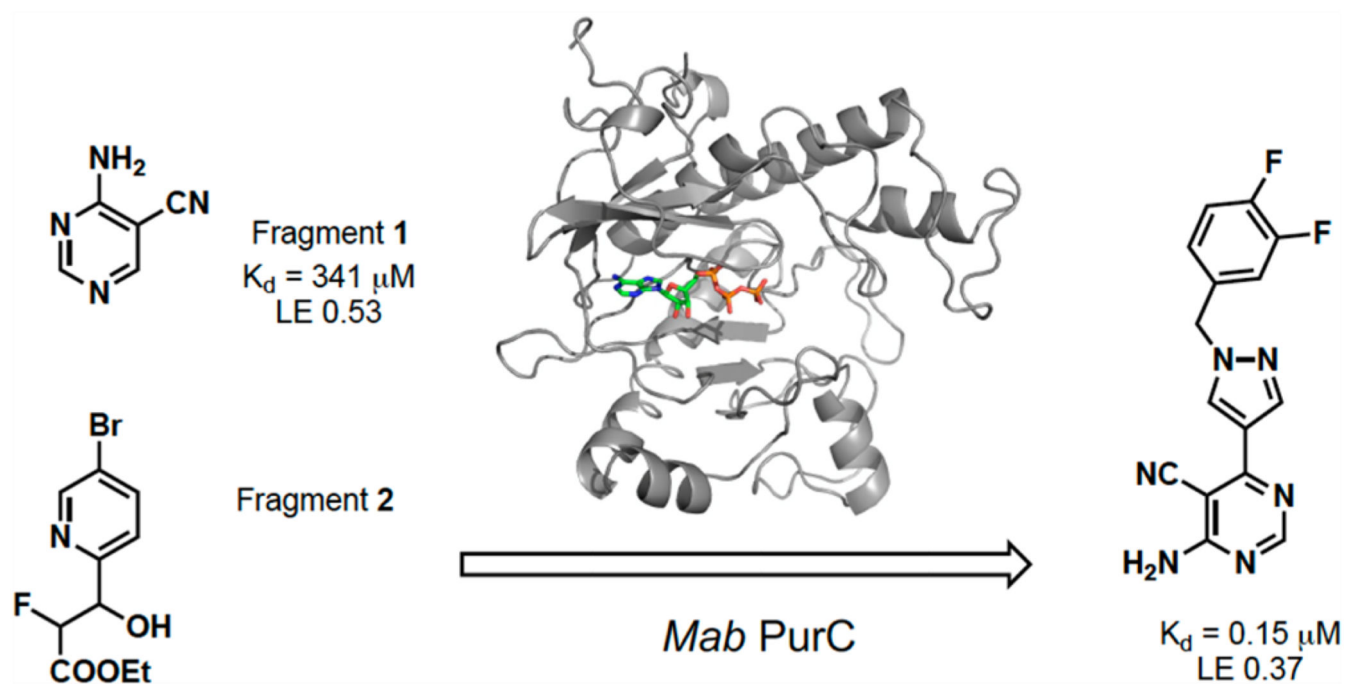
Tom L. Blundell*, Anthony G. Coyne*, Chris Abell

Yusuf Hamied Department of Chemistry, University of Cambridge, Cambridge CB2 1EW, United Kingdom

Abstract

Mycobacterium abscessus (*Mab*) has emerged as a challenging threat to individuals with cystic fibrosis. Infections caused by this pathogen are often impossible to treat due to the intrinsic antibiotic resistance leading to lung malfunction and eventually death. Therefore, there is an urgent need to develop new drugs against novel targets in *Mab* to overcome drug resistance and subsequent treatment failure. In this study, SAICAR synthetase (PurC) from *Mab* was identified as a promising target for novel antibiotics. An in-house fragment library screen and a high-throughput X-ray crystallographic screen of diverse fragment libraries were explored to provide crucial starting points for fragment elaboration. A series of compounds developed from fragment growing and merging strategies, guided by crystallographic information and careful hit-to-lead optimization, have achieved potent nanomolar binding affinity against the enzyme. Some compounds also show a promising inhibitory effect against *Mab* and *Mtb*. This work utilizes a fragment-based design and demonstrates for the first time the potential to develop inhibitors against PurC from *Mab*.

Abstract



Graphic abstract.

Keywords

structure-guided; fragment-based drug discovery; *Mycobacterium abscessus*; cystic fibrosis; PurC; SAICAR synthetase

Mycobacterium abscessus (*Mab*) is a rapidly growing species of nontuberculous mycobacteria (NTM) which is responsible for a wide range of soft tissue infections which have emerged as a major threat to individuals with cystic fibrosis.¹⁻⁴ These infections are often impossible to treat due to their intrinsic antibiotic resistance and result in extremely high treatment failure rates of around 55% despite years of combination chemotherapy and can often prove fatal.⁵⁻⁸ The current drug regimen involves a combination of antibiotics, such as Amikacin, and this may take up to 2 years to be complete. Therefore, there is an urgent need to develop novel drugs targeting *Mab*, as an alternative antibacterial strategy.

Phosphoribosylaminoimidazole succinocarboxamide synthetase or PurC (also known as SAICAR synthetase) is an essential enzyme involved in the *de novo* purine biosynthesis in bacteria and fungi.⁹ The enzyme catalyzes the transformation of 5-aminoimidazole-4-carboxyribonucleotide (CAIR) and L-aspartate to phosphoribosylaminoimidazole-succinocarboxamide (SAICAR) in the presence of adenosine triphosphate (ATP) and Mg^{2+} cofactors (Scheme 1).^{10,11}

It is known that bacteria rely on the *de novo* pathway for their survival, as the pathway plays a crucial role in the synthesis of nucleic acid and nucleotide phosphate precursors for

energy metabolism. Several studies in the past have shown that purine biosynthesis is vital for bacterial growth and persistence in the gut, blood, and lungs.^{12–14}

While most bacterial PurC enzymes exist as homodimers, *Mab* and *Saccharomyces cerevisiae* orthologs function as monomers.^{15–18} In contrast, the human bifunctional ortholog (PAICS) is an octameric enzyme combining a central C-terminal ring of the AIR carboxylase domain and an outer N-terminal SAICAR synthetase domain.¹⁹ A comparison of *Mab* PurC and the SAICAR synthetase domain of the human ortholog shows distinct structural and sequence differences, providing the basis for selective inhibition of this enzyme.²⁰ The structural and functional differences between bacterial PurC and PAICS makes PurC an excellent target for antimicrobial drug discovery.^{15,19,21,22}

Fragment-based drug discovery has emerged as a successful approach for the identification of new drugs. Recently, another drug derived from a fragment-based approach secured a breakthrough approval from the FDA and this methodology is seen as a reliable way forward in small-molecule drug design.²³ Fragments are low-molecular-weight molecules with low structural complexity. The hits that come from a fragment-based screening usually exhibit lower potency than larger molecules identified from a standard high-throughput platform. However, these fragments bind by making high-quality interactions to a hotspot on the biomolecular target leading to highly ligand efficient (LE) molecules.^{24,25}

In this work, the application of a fragment-based approach targeting *Mab* SAICAR synthetase (MabPurC) was used to discover a new class of 4-amino-6-(pyrazol-4-yl)pyrimidine based inhibitors. The fragment elaboration strategies described here utilized the hits identified from both our in-house fragment library and XChem fragment screening facilities as starting points for development.²⁰ Through this study, for the first time, we were able to validate the essentiality of PurC in *Mab* and demonstrate the potential for developing inhibitors against this bacterial enzyme.

■ Results And Discussion

Generation of purC Gene Knockout Mutants

In order to assess the suitability of targeting PurC for antimicrobial drug development, essentiality studies of PurC in *Mab* were performed. This approach made use of a recombineering system to generate knockout mutants in *M. abscessus subsp. massiliense*. The resulting knockouts were analyzed by PCR and compared with that of the wild-type. The knockout strains did not grow in normal growth media, but colonies appeared when the media was supplemented with hypoxanthine, thus supporting the essentiality of the *purC* gene in bacterial growth and replication (Figure 1).

Initial SAR Studies

Research within our group has identified several fragments that were found to bind into the adenine pocket of the ATP binding site of *M. abscessus* PurC. These were characterized using a range of biophysical techniques, including differential scanning fluorimetry (DSF), isothermal titration calorimetry (ITC), and X-ray crystallography.²⁰ The fragment hits were identified using a dual strategy, first, the screening of an in-house fragment library

of 960 fragments and, second, the screening of two diverse fragment libraries (125 and 768 fragments) at the XChem screening platform at the Diamond Light Source. The screening of the in-house fragment library led to the identification of eight fragments which were characterized using a range of biophysical techniques and X-ray crystallography. The screening of the two fragment libraries at XChem led to the identification of thirty five fragments, of which 60% of these were shown to bind at the ATP site by X-ray crystallography. However, no biophysical data was available for these fragments. One of the hits identified from the screening of the in-house fragment library was 4-amino-5-pyrimidine-carbonitrile, fragment **1**. The X-ray crystal structure of *MabPurC* in complex with this fragment shows several key interactions which include (i) H-bonding of the amino moiety of **1** to the His69 side chain and to the main chain carbonyl of R91, (ii) H-bonding of the N3 of pyrimidine to the amide nitrogen of Leu93, and (iii) H-bonding of the nitrile nitrogen to the amide nitrogen of D213. These interactions are also made by the adenine ring of ATP when it binds to PurC. Along with its well-characterized interactions, this fragment also demonstrated a T_m of +3.6 °C and a K_d value of 340 μM (for ATP; K_d = 88 μM).

A further fragment screen was also performed on *MabPurC* with a more structurally diverse library using the high-throughput X-ray screening approach (XChem) available at the Diamond Light Source.²⁶ With the access to the roboticized XChem facility,^{27–30} fragment **2** (XC1) was identified and its binding interactions to *MabPurC* were characterized (Figure 2).²⁰ One of the distinct interactions that this fragment makes is the π -interaction between the pyridine ring of fragment **2** and the side chain of R17. The movement of the Arg side chain to accommodate the pyridine ring of fragment **2** was not previously observed from our in-house fragment screening and is not observed in the ATP-bound structure (PDB code 6YX3; Figure 2f). The flexibility of this R17 side chain was identified as beneficial towards further medicinal chemistry intervention to design chemical scaffolds that possess a slightly different mode of binding to that of ATP. This important aspect was therefore incorporated into a fragment-growing strategy from the ATP binding site.

Prior to hit-to-lead elaboration, further DSF was performed on a number of close analogues of fragment **1** to examine preliminary SAR around the pyrimidine pharmacophore. As shown in Table 1, a comparison between fragment **1** (K_d = 341 μM , LE 0.53) and compound **4** (K_d = 1060 μM , LE 0.45) shows that the pyrimidine analogue exhibits a higher T_m and a 3-fold increase in the binding affinity compared to pyridine counterparts. The addition of a chlorine atom at the 6-position of the pyrimidine ring is tolerated as shown in compound **3** (K_d = 159 μM , LE 0.52) when compared to the original fragment **1**. The replacement of a nitrile with a chlorine atom (compounds **3** vs **6**) decreases T_m and shows a slight decrease in binding affinity (for compound **6**; K_d = 442 μM , LE 0.51). This substitution could be beneficial for fine-tuning the physicochemical properties of a lead compound later in the optimization as compounds with a chlorine substituent show a higher clogP and lower PSA compared to compounds with a nitrile functional group.³¹ However, the removal of H-bond acceptor at this position (CN or Cl) diminishes the change in the melt-temperature (T_m) completely as seen in compound **8**. This shows the significance of having a H-bonding acceptor present at the 5-position of pyrimidine. The change to the ring to a pyrazine ring

5 and the removal of N1 in pyrimidine **4** and **7** and removal of the cyano-group in the 5-position **8** all had a detrimental effect on the T_m .

Hit-to-Lead Optimization

Fragment **1** was selected for further elaboration due to it having the highest ligand efficiency (LE) in the series. A closer examination of the X-ray crystal structure of fragment **1** with *MabPurC* reveals a vector for elaboration, into the “ribose binding pocket”, at the 6-position of the pyrimidine, which could be explored as an area for fragment growth as it is tolerated as seen in compound **3**. Utilizing fragment elaboration at this position would allow the possibility of adding the feature of the pyridine moiety of fragment **2** into fragment **1**. These two fragments are almost perpendicular to each other, and therefore it is necessary that a flexible linker be identified to join them together.

As shown in Table 2, the addition of a 4-pyrazolyl moiety effectively enhanced the binding affinity by an order of magnitude, resulting in the identification of compound **9** ($K_d = 23 \mu\text{M}$, LE 0.39). Even though the X-ray crystal structure of *MabPurC* in complex with compound **9** shows that the pyrazole does not make any significant polar interactions to *MabPurC* as demonstrated in Figure 3b, all the original polar contacts of the pyrimidine core have been retained. It is worth noting that the attached pyrazole **9** or pyridine (compounds **10** and **11**) and the pyrimidine core align in a coplanar fashion (Figure 3).

Following the identification of compound **9**, guided by the structural information, various flexible groups and saturated side chains were examined in order to identify the best substituent to incorporate (Table 3). The morpholine ring was employed in a number of analogues, **12**, **13**, and **15**, to assist with the solubility of the compounds. The compound **14** ($K_d = 22 \mu\text{M}$, LE 0.32) which has an ethyl ester side chain was chosen, and although an increase in its binding affinity was not observed, the added hydrophobic ethyl ester was identified by X-ray crystallography close to the region where the pyridine moiety of fragment **2** is located, Figure 3d. A similar binding mode was also observed in the X-ray crystal structure of **13** ($K_d = 52 \mu\text{M}$, LE 0.26), Figure 3c. Interestingly, the ethyl morpholine group in **13** occupies almost the same site as the pyridine in fragment **2**. Even though these two compounds (**14** and **13**) did not show further improvement in binding affinity to *MabPurC*, the corresponding X-ray crystal structures have provided the critical information necessary for further fragment optimization (Figure 3c and d).

On the basis of the X-ray crystal structure of *MabPurC* in complex with compound **13**, it was proposed that the incorporation of the 3-pyridylmethyl moiety at the N1 of the pyrazole ring would mimic the compound characteristics that engage the π -interaction seen with the pyridine moiety of fragment **2**. The resulting compound **16** ($K_d = 3.1 \mu\text{M}$, LE 0.36) shows an order of magnitude increase in its binding affinity compared to compound **13**. The alignment of this pyridine ring of compound **16** in the *MabPurC* binding site by forming π -stacking interaction to R17 side chain is crucial for the enhanced affinity observed (Figure 3e, Table 3).

Various substituted phenyl and pyridyl rings were examined to investigate the effect of the aromatic rings in forming the π interaction to R17. It is generally accepted that

fluorobenzene is a good isostere of pyridine due to the similarity in dipole and electron density.³² There are many successful examples of an aryl C–F mimicking an azine nitrogen atom in drug discovery.³³ This change is also deemed as a way to modulate the physicochemical properties of the compound as removing a nitrogen atom will reduce the compound's basicity and increase its clogP at the same time. A number of analogues were synthesized, including pyridylmethyl and fluorobenzyl side chains. Compound **19** ($K_d = 0.25 \mu\text{M}$, LE 0.41) featuring a 3-fluorophenyl moiety shows another order of magnitude improvement in binding affinity while all key interactions to *Mab*PurC are still observed in the corresponding X-ray crystal structure, Figure 4a.

The modulation of the electronic nature of this aryl ring in compound **19** is crucial to the affinity jump observed, and various substituted phenyl analogues with electron-withdrawing and electron-donating groups were subsequently synthesized to test this hypothesis. The fluorine substituted compounds **22** ($K_d = 0.22 \mu\text{M}$, LE 0.41) and **27** ($K_d = 0.15 \mu\text{M}$, LE 0.37), Figure 4c, retain a strong binding affinity as observed in compound **19**. Interestingly, compound **23**, possessing an unsubstituted phenyl ring, also gave a $K_d = 0.28 \mu\text{M}$, with an LE of 0.43. Compound **24** ($K_d = 0.53 \mu\text{M}$, LE 0.38) where a methyl group was introduced on the methylene carbon, a derivative of compound **23**, also displays a good affinity, suggesting that this modification is tolerated, and this could possibly offer a further vector for elaboration, Figure 4b.

The fragment SAR (Table 1) had shown that the interchange between the CN and Cl moieties is tolerated and the removal of the N1 atom in pyrimidine has a dramatic negative effect on binding affinity. As shown in Table 3, each compound (**28**, **29**, **30**, and **31**) shares the same 3-fluorophenyl side chain as **19** but with a slightly different core structure. Compound **28** ($K_d = 0.35 \mu\text{M}$, LE 0.39) possessing a chlorine atom at the 5-position of pyrimidine rather than a nitrile group, exhibits a similar binding affinity as compared to **19** (Figure 4d), whereas compounds **29** and **30** led to a decrease in binding affinities. This observation corresponds to the results observed in early fragment SARs and could be important for further optimization, as the derivatives containing a Cl substituent would possess a higher lipophilicity in comparison to compounds having a CN moiety and therefore could play additional roles in determining compound permeability and retention in the mycobacteria

Phenotypic Screening of Compounds against *Mab* and *Mtb*

The minimal inhibitory concentrations (MIC) of the selected compounds with $K_d < 50 \mu\text{M}$ were determined for both *M. abscessus* and *M. tuberculosis in vitro* (Table 4). The compounds were screened against *Mtb* as there is an overall percentage identity between the *Mab* and *Mtb* PurC orthologues of 75%. The important active site residues and those involved in the interactions with the compounds described above are 100% conserved between *Mab* and *Mtb* PurC (see Figure S7). Almost all of the compounds elaborated from the fragments exhibited complete growth inhibition at 50–200 μM against *Mab*. Whereas the compounds exhibited growth inhibition of 50 μM against *Mtb*, compounds **28** and **29** showed more promising inhibitory activity at 25 μM against *Mtb* (Table 3). The lack of significant MIC against *Mab* and *Mtb* shows the challenges of developing small molecules

against mycobacteria. This lack of activity could be due to a number of factors. For example *Mab* has been shown to have a large number of efflux pumps, and any small molecules which get across the cell wall could be effluxed back out through these. In order to understand whether the compounds were getting across the *Mab* cell wall and engaging with PurC, hypoxanthine rescue experiments were carried out. Hypo-xanthine can be used as a salvage pathway of purine biosynthesis where this is converted to inosine monophosphate (IMP) by hypoxanthine-guanine phosphoribosyltransferase (HGPRT; Scheme 1). Compound **19** was examined with varying concentrations of hypoxanthine (Figure S8); however the results were inconclusive. While there seems to be rescue at a concentration of 200 μM , this is at the limit of the MIC measured. The chemotypes which have been identified that get into *Mab* tend to vary significantly. Many of the current antibiotics used to treat *Mab* infections have a log *P* less than zero (for example the aminoglycoside Amikacin) and many of these are highly hydrophilic. However, small molecule inhibitors (for example, those targeting Mmp13 from *Mab*) which have been developed and show measurable effects on mycobacteria tend to have a log *P* > 4.³⁴ The compounds that were developed in this work have log *P* values which range from -1.6 to 2.2, which could possibly explain the lack of activity on *Mab*.

Further work is currently ongoing first to further optimize the compounds developed and second to understand how these compounds engage with PurC within *Mab*.

Synthetic Chemistry

The early compounds in the series were synthesized following the routes shown in Scheme 2. Compounds **9**, **10**, and **11** were synthesized using a Suzuki coupling reaction between pyrazole boronic acid **32** or pyridine boronic acids **33** and **34** and 4-amino-6-chloropyrimidine-5-carbonitrile **3** using Pd(*t*-Bu₃P)₂ as a catalyst in the presence of KF to afford the desired products. These were obtained in moderate to good yields (69% yield for **9**, 25% for **10**, and 24% for **11**).³⁵ Compound **12** was synthesized from its corresponding 4-iodopyrazole **35** and 4-morpholinecarbonyl chloride to afford compound **36**. This then underwent a Miyaura borylation reaction using B₂pin₂ in the presence of a Pd(dppf)Cl₂ catalyst to yield the boronate ester **37** in good yield (53%).³⁶ The boronate ester **37** was then reacted with the 4-amino-6-chloropyrimidine-5-carbonitrile **3** heterocycle using Suzuki reaction conditions (Pd(*t*-Bu₃P)₂, KF, under MW irradiation, 150 °C over 40 min) to obtain **12** in 37% yield. Compounds **13**, **14**, and **15** were synthesized from the corresponding pyrazole boronate esters and 4-amino-6-chloropyrimidine-5-carbonitrile under the Suzuki reaction conditions to yield the products in moderate yields (32% yield for **13**, 38% for **14**, and 19% for **15**).³⁶

For most of the final products in the series (**16–31**), as depicted in Scheme 3, the synthesis began with the substitution reaction between pyrazole-4-boronic acid pinacol ester and an alkyl halide of choice (**39–50**) in the presence of a carbonate base (Cs₂CO₃ or K₂CO₃) to obtain the corresponding N-alkylated pyrazole boronate esters (**51–62**) in moderate to good yields (31% to quantitative yield).³⁷ The Suzuki coupling reactions under the same conditions as described previously using Pd(*t*-Bu₃P)₂ as a catalyst were employed in the preparation of the final compounds, resulting in 20–81% yield of the desired products.

Compound **7** was prepared according to the reported literature procedure starting from the bromination reaction of 4-methoxy-2-pyridone using phosphorus oxybromide (POBr₃) followed by nucleophilic amination using aqueous ammonia to replace the bromine at the 2-position of pyridine.³⁸ Compound **29** was synthesized using the same conditions as those for the Suzuki coupling reaction between previously prepared compound **54** and compound **7** in 61% yield. The synthesis of **30** began with the Suzuki coupling reaction between **54** and 2,3-dichloro-4-iodopyridine **65**. The reaction proceeded in a 56% yield of **66** with the 4-iodo moiety being replaced with a pyrazole side chain. Compound **66** underwent a palladium-catalyzed Buchwald–Hartwig reaction with benzophenone imine, and the imine product obtained was then hydrolyzed *in situ* under acidic conditions using 1 M HCl to afford the desired 2-aminopyridine **30** (63% yields over two steps).³⁹

■ Conclusion

The application of a fragment-based approach towards the discovery of novel inhibitors of *M. abscessus* PurC is described. A combination of in-house fragment screening and high-throughput X-ray crystallographic screening provided crucial starting points for the fragment elaboration process. The fragment growing and merging strategies combined the structural characteristics of the two parent fragments, fragment **1** and fragment **2**. The hit-to-lead elaboration, guided by X-ray crystallographic information and binding affinity data, resulted in the identification of compound **19** ($K_d = 50$ nM, LE 0.41) and compound **27** ($K_d = 150$ nM, LE 0.39) both possessing promising *in vitro* binding affinities. The fragment growing and merging approaches described further demonstrate the strength of fragment-based design in accelerating the overall hit-to-lead progression. These results are encouraging and this study, as a first example of designing inhibitors against bacterial PurC, shows the potential for developing novel antimicrobials targeting this enzyme. However, this study also highlights the challenges in developing small molecules against targets in *M. abscessus*. While small molecules with high affinities can be developed using the fragment-based approach, the challenge is ensuring that these inhibitors get across the cell wall of *M. abscessus* and engage with the target *in vivo*. Work is currently underway to improve the overall physicochemical profiles of the lead compounds described herein in order to enhance their affinity against *M. abscessus*.

■ Methods

The characterization data for all of the compounds described can be found in the Supporting Information.

***Mycobacterium abscessus* purC gene Knockout Studies**

Deletion of *purC* gene from *M. abscessus subsp massiliense* CIP108297 was carried out by recombineering as described previously. Briefly, primers were designed to amplify 1000 bp flanking regions upstream and downstream of the gene. A streptomycin cassette obtained from pHP45W was cloned between these fragments to create an allelic exchange substrate (AES). *M. abscessus subsp massiliense* containing a modified version of pJV53 with the *xyIE* gene (pJV53-*xyIE*) was induced for 4 h with 0.2% acetamide and electroporated

with 500 ng of AES. Cells were incubated at 37 °C overnight and plated on 7H11 ADC containing streptomycin 200 mg/mL for selection and hypoxanthine 20 mg/mL to complement growth of the mutant. After 5 days colonies were picked on plates with or without hypoxanthine and checked by PCR to confirm deletion of the gene.

Amplification of *purC* Gene from *Mycobacterium abscessus* Genomic DNA

Genomic DNA sample was obtained from *Mycobacterium abscessus* (ATCC 19977). The stock of genomic DNA (6 ng/mL) was diluted using sterile water to make a working concentration of 0.6 ng/mL. The *purC* gene (MAB_0689) was amplified using the following primers (Sigma):

Forward Primer: 5'-ATTCCATGGTGCGTCCTTCG-CTGTCCGATTAC-3'

Reverse Primer: 5'-TATCTCGAGTCACGCCGACG-GGCCAATCC-3'

The following thermocycle program was used: stage 1 × 1 cycle, activation of polymerase at 95 °C for 2 min; stage 2 × 35 cycles, denaturation at 95 °C for 20 s, annealing at 70 °C for 20 s, extension at 70 °C for 45 s. This was followed by stage 3, final extension at 70 °C for 10 min.

Molecular Cloning

The purified PCR product and a PHAT2 *E. coli* expression vector containing Amp^r and noncleavable N-terminal His-tag were then subjected to restriction digestion with NcoI and XhoI restriction endonucleases (ThermoScientific). The ligation of the digested insert and vector was performed using T4 DNA ligase (New England Biolabs), by incubation at room temperature for 10 min. The ligation product was transformed into *E. coli* DH5a competent cells by the heat-shock method and plated on LB agar-kanamycin plates and incubated at 37 °C. Single colonies were randomly picked on the following day and inoculated in LB media with kanamycin (30 mg/mL) and grown overnight at 37 °C. Plasmids from the resulting cultures were isolated and purified (ThermoScientific GeneJet Plasmid Miniprep Kit). The integrity of the clones was confirmed by sequencing (DNA Sequencing Facility, Department of Biochemistry, University of Cambridge, UK).

Expression and Purification of PurC Protein

E. coli BL21 (DE3) strains containing N-His-PurC PHAT2 plasmids were grown overnight at 37 °C in LB-media containing Ampicillin (100 µg/mL). This seed-stage culture was used to inoculate six shake flasks containing 1 L each of 2XYT media with Ampicillin (100 µg/mL) until the optical density ($A_{600\text{nm}}$) reached 0.6. Expression of the recombinant construct was induced by the addition of isopropyl β -D-1-thiogalactopyrano-side (IPTG) to a final concentration of 0.5 mM and further allowed to grow at 18 °C for 16 h. Cells were harvested by centrifugation at 4 °C for 20 min at 5000g, and the pellet was resuspended in buffer A (50 mM Tris-HCl pH 7.5, 350 mM NaCl, 20 mM Imidazole). Then, 10 µg/mL of DNaseI, 5 mM MgCl₂, and protease inhibitor cocktail tablets (New England Biolabs) were added to the cell suspension. The cells were lysed by sonication (Branson), and the lysate was clarified by centrifugation at 4 °C for 40 min at 25 568 g. The clarified lysate was

filtered using a 0.45 μm syringe filter and passed through a pre-equilibrated (with buffer A) 10 mL prepacked nickel-sepharose column (HiTrap IMAC FF, GE Healthcare). The column was washed with five column volumes of buffer A, and the bound protein was eluted as 2×12 mL elutes using buffer B (50 mM Tris-HCl pH 7.5, 350 mM NaCl, and 500 mM imidazole). The protein was analyzed on a 15% SDS-PAGE gel, and elutes from the HiTrap IMAC column containing the sample protein were pooled and subjected to dialysis against 2 L of buffer C (50 mM Tris-HCl pH 7.5, 350 mM NaCl) overnight at 4 °C. After overnight dialysis, the protein was concentrated using a 10 kDa centrifugal concentrator (Sartorius Stedim) and loaded onto a pre-equilibrated (with buffer D: 50 mM Tris-HCl, pH 7.5, 150 mM NaCl) 120 mL Superdex200 16/600 column (GE Healthcare). Two milliliter fractions were collected and analyzed on a 15% SDS-PAGE gel, followed by MALDI-Mass fingerprinting. Fractions corresponding to pure PurC protein were pooled, concentrated to 26 mg/mL, flash frozen in liquid nitrogen, and stored at -80 °C.

Crystallization of *M. abscessus* PurC

Screening of commercial sparse matrix libraries for the identification of appropriate crystallization conditions for *M. abscessus* PurC protein was performed as described previously.²⁰ Drops containing 18 mg/mL of the protein in storage buffer (50 mM Tris-HCl pH 7.5, 150 mM NaCl) and reservoir were set up at drop ratios of 1:1 and 2:1 (of protein/reservoir, respectively) using a Mosquito crystallization robot (TTP labtech), in 96-well sitting drop plates. The drops were equilibrated against 80 μL of the corresponding reservoir solution at 19 °C. The best diffracting crystals were observed in the crystal condition containing 0.2 M LiSO_4 , 0.1 M Bis-Tris pH 5.5, and 25% PEG 3350.

Soaking of Fragments and Compounds on PurC Native Crystals

Crystals for soaking were grown at 19 °C in 48-well sitting drop plates in a grid consisting of 0.2 M lithium sulfate, 21–28% PEG 3350, and 0.1 M Bis-Tris pH 5.5–6.5, set up at drop ratios of 1:1 μL (of protein and reservoir, respectively). The crystals appeared in 3–5 days and were then moved into 24-well hanging drop plates to allow soaking in 4 μL drops containing the respective reservoir solutions and 10 mM fragments/compounds. The drops were then equilibrated against 800 μL of the respective reservoir solution for 16 h at 19 °C in 24-well hanging drop plates.

Co-crystallization of PurC Protein with ATP and Lead Compounds

For cocrystallization of PurC, 18 mg/mL of the protein was mixed with a 2–5 mM final concentration of the ligand/compound and incubated for 2 h on ice. The crystallization drops were set up using the incubated samples at a protein to reservoir drop ratio of 0.3:0.3 μL , in 96-well (MRC2) sitting drop plates in 0.2 M lithium sulfate, 21–28% PEG 3350, 0.1 M Bis-Tris at a pH of 5.5–6.5. The drops were equilibrated against 70 μL of reservoir at 19 °C.

X-ray Data Collection and Processing

The crystals were flash-cooled in cryo-solution consisting of 25% ethylene glycol in the corresponding reservoir. X-ray data sets were collected at the Diamond Light Source in the UK, using the rotation method at a wavelength of 0.979 Å; omega start, 0°; omega

oscillation, 0.15°; total images, 2100–2400; exposure time, 0.05–0.08 s, and at the French National Synchrotron facility (Soleil), at a wavelength of 0.979 Å; omega start, 0°; omega oscillation, 1°; total oscillation, 210–240°; exposure time, 0.5 s. The diffraction images were processed using AutoPROC,⁴⁰ utilizing XDS⁴¹ for indexing and integration, and POINTLESS,⁴² AIMLESS,⁴³ and TRUNCATE⁴⁴ programs from the CCP4 Suite⁴⁵ for data reduction, scaling, and calculation of structure factor amplitudes and intensity statistics. PurC ligand bound structures were solved by molecular replacement using PHASER⁴⁶ with the atomic coordinates of the *Mycobacterium abscessus* PurC apo structure as a search model, as described previously.²⁰ Structures were refined using REFMAC⁴⁷ and PHENIX.⁴⁸ Model building was performed using the COOT⁴⁹ interactive graphics program, and electron density maps were calculated with $2|F_o| - |F_c|$ and $|F_o| - |F_c|$ coefficients. OMIT difference maps $|mF_o - DF_c|$ ⁵⁰ were calculated and analyzed to verify positions of modelled ligands.

Thermal Shift Assay

Reactions were carried out in triplicate in a 96-well plate. Each reaction contained a final concentration of 20 μM PurC, 5 × SYPRO Orange, 100 mM HEPES at pH 7.5, 150 mM NaCl, 1 mM MgCl₂, 5% DMSO, and 5 mM compounds **1–3** and **5–8**. Compound **4** was screened at a concentration of 3 mM, and all other compounds were screened at a concentration of 1 mM. The plate was centrifuged briefly to remove bubbles and analyzed in a Bio-Rad CFX96 Touch or CFX Connect RT-qPCR machine. Samples were incubated at 25 °C for 10 min, and the temperature was then raised to 96 °C at a rate of 1 °C min⁻¹ while fluorescence was recorded with excitation/emission wavelengths of 490/575 nm. Data were analyzed in Microsoft Excel to calculate the melting temperature (T_m) and T_m for each condition relative to the protein and DMSO-only control.

Isothermal Titration Calorimetry

ITC experiments were carried out in a buffer of 100 mM HEPES at pH 7.5, 150 mM NaCl, and 1 mM MgCl₂. Protein was dialyzed against this buffer overnight before experiments and subsequent dilutions of protein and ligands used the remaining dialysis buffer. Generally, ligands at a concentration of 4 mM (ATP and CAIR), 2–5 mM (fragments and weakly binding compounds), or 0.2–1.5 mM (strongly binding compounds) were titrated against 20–100 μM PurC in a Malvern MicroCal iTC200 machine. To correct for enthalpy of dilution, ligands were also titrated against a buffer and the peak values of this run subtracted from the experimental run as a reference. When ligands were dissolved in DMSO, an appropriate concentration of DMSO (5–10% v/v) was added to other solutions. Data were analyzed using the Origin software (OriginLab, Northampton, MA, USA). The titration of an initial injection (0.2 μL) was discarded during data processing.

Phenotypic Screening against *Mab*

M. abscessus subspecies *abscessus* (ATCC19977) was transformed with pmv310 plasmid expressing Lux ABDCE operon, grown in Middlebrook 7H9 broth supplemented with ADC (Sigma, UK). Minimum inhibitory concentrations (MIC) were determined according to the Clinical and Laboratory Standards Institute (CLSI) method M07-A9. *Mycobacteria* were grown to an OD₆₀₀ of 0.2–0.3 (Jenway 6300 spectrophotometer) in liquid culture, and

1×10^5 bacteria were added to each well of 96-well plates containing serial dilutions of compounds (400, 200, 100, 50, 25, 12.5, 6.3, 3.1, 1.6, 0.8, 0.4, 0 μM), in triplicate wells per condition, and incubated at 37 °C until growth was seen in the control wells. The MIC value was determined as the last well which showed no bacterial growth.

Supplementary Material

Refer to Web version on PubMed Central for supplementary material.

Acknowledgments

This paper is dedicated to the memory of Professor Chris Abell, who passed away on October 26th, 2020. The authors would like to thank the Diamond Light Source for beam-time (proposals mx9537, mx14043, mx18548) and the staff of beamlines I03, I02, I04, I04-1, and I24 and the French National Synchrotron facility (Soleil) for assistance with data collection. The authors are grateful to Prof. Frank von Delft, Dr. Patrick Collins, and the XChem team at the DLS I04-1 beamline for access to fragment libraries and the high-throughput fragment screening facility. We thank Prof. Adam Nelson and his group at the University of Leeds for the three-dimensional fragment library at the DLS XChem facility. S.E.T. was funded by the Cystic Fibrosis Trust and Fondation Botnar (Grant No. 6063). S.C. and S.G.G. were funded by the Fondation Botnar (Grant No. 6063). A.W. was funded by the EPSRC. R.A.F. is funded by the Cystic Fibrosis Trust Strategic Research Centre (SRC010) and Innovation Hub (IH01) awards, Wellcome Trust (I07032AIA), and Royal Papworth Hospital Research Award. V.M. was funded by the Bill and Melinda Gates Foundation SHORTEN-TB (OPP1158806). T.L.B. is funded by the Wellcome Trust (Investigator Award 200814_Z_16_Z). M.J. and J.M.B. are funded by the Cystic Fibrosis Strategic Research Centre (SRC010), M.A.G.d.E. is funded by the American Leprosy Mission (G88726).

Abbreviations

■	
SAICAR	phosphoribosylaminoimidazole-succinocarboxamide
Mab	<i>Mycobacterium abscessus</i>
Mtb	<i>Mycobacterium tuberculosis</i>
DSF	differential scanning fluorimetry
ITC	isothermal titration calorimetry
SAR	structure activity relationship
PSA	polar surface area
LE	ligand efficiency

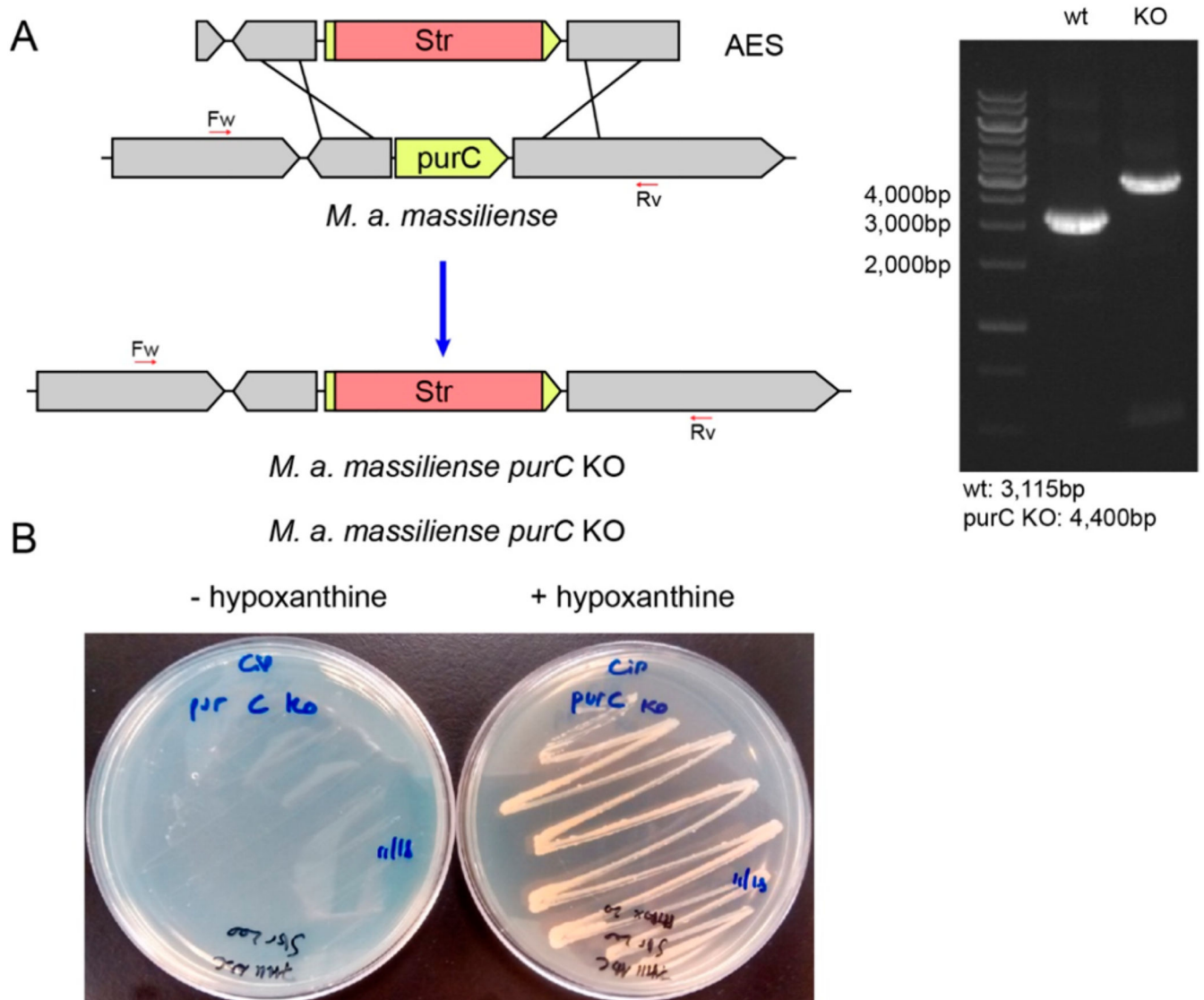
References

- (1). Liu H, Dong F, Liu J, Liu J, Pang Y, Zhao S, Lu J, Li H. Successful management of *Mycobacterium abscessus* complex lung disease in an otherwise healthy infant. *Infect Drug Resist.* 2019; 12: 1277–1283. [PubMed: 31190915]
- (2). Esther CR Jr, Esserman DA, Gilligan P, Kerr A, Noone PG. Chronic *Mycobacterium abscessus* infection and lung function decline in cystic fibrosis. *J Cyst Fibros.* 2010; 9 (2) 117–23. [PubMed: 20071249]
- (3). Bar-On O, Mussaffi H, Mei-Zahav M, Prais D, Steuer G, Stafler P, Hananya S, Blau H. Increasing nontuberculous mycobacteria infection in cystic fibrosis. *J Cyst Fibros.* 2015; 14 (1) 53–62. [PubMed: 24917112]

- (4). Qvist T, Taylor-Robinson D, Waldmann E, Olesen HV, Hansen CR, Mathiesen IH, Hoiby N, Katzenstein TL, Smyth RL, Diggle PJ, Pressler T. Comparing the harmful effects of nontuberculous mycobacteria and Gram negative bacteria on lung function in patients with cystic fibrosis. *J Cyst Fibros.* 2016; 15: 380–5. [PubMed: 26482717]
- (5). Chen J, Zhao L, Mao Y, Ye M, Guo Q, Zhang Y, Xu L, Zhang Z, Li B, Chu H. Clinical Efficacy and Adverse Effects of Antibiotics Used to Treat *Mycobacterium abscessus* Pulmonary Disease. *Front Microbiol.* 2019; 10: 1977. [PubMed: 31507579]
- (6). Sfeir M, Walsh M, Rosa R, Aragon L, Liu SY, Cleary T, Worley M, Frederick C, Abbo LM. *Mycobacterium abscessus* Complex Infections: A Retrospective Cohort Study. *Open Forum Infect Dis.* 2018; 5 (2) ofy022 [PubMed: 29450214]
- (7). Raats D, Lorent N, Saegeman V, Vos R, van Ingen J, Verleden G, Van Raemdonck D, Dupont L. Successful lung transplantation for chronic *Mycobacterium abscessus* infection in advanced cystic fibrosis, a case series. *Transpl Infect Dis.* 2019; 21 (2) e13046 [PubMed: 30597699]
- (8). Osmani M, Sotello D, Alvarez S, Odell JA, Thomas M. *Mycobacterium abscessus* infections in lung transplant recipients: 15-year experience from a single institution. *Transpl Infect Dis.* 2018; 20 (2) e12835 [PubMed: 29359872]
- (9). Moffatt BA, Ashihara H. Purine and pyrimidine nucleotide synthesis and metabolism. *Arabidopsis Book.* 2002; 1 e0018 [PubMed: 22303196]
- (10). Manjunath K, Jeyakanthan J, Sekar K. Catalytic pathway, substrate binding and stability in SAICAR synthetase: A structure and molecular dynamics study. *J Struct Biol.* 2015; 191 (1) 22–31. [PubMed: 26072057]
- (11). Tuntland ML, Fung LW. Substrate independent ATPase activity may complicate high throughput screening. *Anal Biochem.* 2016; 510: 18–20. [PubMed: 27430931]
- (12). Samant S, Lee H, Ghassemi M, Chen J, Cook JL, Mankin AS, Neyfakh AA. Nucleotide biosynthesis is critical for growth of bacteria in human blood. *PLoS Pathog.* 2008; 4 (2) e37 [PubMed: 18282099]
- (13). Vogel-Scheel J, Alpert C, Engst W, Loh G, Blaut M. Requirement of purine and pyrimidine synthesis for colonization of the mouse intestine by *Escherichia coli*. *Appl Environ Microbiol.* 2010; 76 (15) 5181–7. [PubMed: 20562286]
- (14). Wang N, Ozer EA, Mandel MJ, Hauser AR. Genomewide identification of *Acinetobacter baumannii* genes necessary for persistence in the lung. *MBio.* 2014; 5 (3) e01163-14 [PubMed: 24895306]
- (15). Ginder ND, Binkowski DJ, Fromm HJ, Honzatko RB. Nucleotide complexes of *Escherichia coli* phosphoribosylaminoimidazole succinocarboxamide synthetase. *J Biol Chem.* 2006; 281 (30) 20680–8. [PubMed: 16687397]
- (16). Levdikov VM, Barynin VV, Grebenko AI, Melik-Adamyanyan WR, Lamzin VS, Wilson KS. The structure of SAICAR synthase: an enzyme in the de novo pathway of purine nucleotide biosynthesis. *Structure.* 1998; 6 (3) 363–76. [PubMed: 9551557]
- (17). Wolf NM, Abad-Zapatero C, Johnson ME, Fung LW. Structures of SAICAR synthetase (PurC) from *Streptococcus pneumoniae* with ADP, Mg²⁺, AIR and Asp. *Acta crystallographica. Section D, Biological crystallography.* 2014; 70 (3) 841–50.
- (18). Zhang R, Skarina T, Evdokimova E, Edwards A, Savchenko A, Laskowski R, Cuff ME, Joachimiak A. Structure of SAICAR synthase from *Thermotoga maritima* at 2.2 angstroms reveals an unusual covalent dimer. *Acta crystallographica Section F, Structural biology and crystallization communications.* 2006; 62 (4) 335–339. [PubMed: 16582479]
- (19). Li SX, Tong YP, Xie XC, Wang QH, Zhou HN, Han Y, Zhang ZY, Gao W, Li SG, Zhang XC, Bi RC. Octameric structure of the human bifunctional enzyme PAICS in purine biosynthesis. *J Mol Biol.* 2007; 366 (5) 1603–14. [PubMed: 17224163]
- (20). Thomas SE, Collins P, James RH, Mendes V, Charoensutthivarakul S, Radoux C, Abell C, Coyne AG, Floto RA, von Delft F, Blundell TL. Structure-guided fragment-based drug discovery at the synchrotron: screening binding sites and correlations with hotspot mapping. *Philos Trans A Math Phys Eng Sci.* 2019; 377 (2147) 20180422 [PubMed: 31030650]
- (21). Ducati RG, Breda A, Basso LA, Santos DS. Purine Salvage Pathway in *Mycobacterium tuberculosis*. *Curr Med Chem.* 2011; 18 (9) 1258–75. [PubMed: 21366536]

- (22). Wolf NM, Abad-Zapatero C, Johnson ME, Fung LWM. Structures of SAICAR synthetase (PurC) from *Streptococcus pneumoniae* with ADP, Mg²⁺, AIR and Asp. *Acta Crystallographica Section D Biological Crystallography*. 2014; 70 (3) 841–850. [PubMed: 24598753]
- (23). Murray CW, Newell DR, Angibaud P. A successful collaboration between academia, biotech and pharma led to discovery of erdafitinib, a selective FGFR inhibitor recently approved by the FDA. *Med Chem Comm*. 2019; 10 (9) 1509–1511.
- (24). Mendes V, Blundell TL. Targeting tuberculosis using structure-guided fragment-based drug design. *Drug Discovery Today*. 2017; 22 (3) 546–554. [PubMed: 27742535]
- (25). Scott DE, Coyne AG, Hudson SA, Abell C. Fragmentbased approaches in drug discovery and chemical biology. *Biochemistry*. 2012; 51 (25) 4990–5003. [PubMed: 22697260]
- (26). Collins PM, Douangamath A, Talon R, Dias A, Brandao-Neto J, Krojer T, von Delft F. Achieving a good crystal system for crystallographic X-Ray fragment screening. *Methods Enzymol*. 2018; 610: 251–264. [PubMed: 30390801]
- (27). Pearce NM, Krojer T, Bradley AR, Collins P, Nowak RP, Talon R, Marsden BD, Kelm S, Shi J, Deane CM, von Delft F. A multi-crystal method for extracting obscured crystallographic states from conventionally uninterpretable electron density. *Nat Commun*. 2017; 8 15123 [PubMed: 28436492]
- (28). Krojer T, Talon R, Pearce N, Collins P, Douangamath A, Brandao-Neto J, Dias A, Marsden B, von Delft F. The XChemExplorer graphical workflow tool for routine or large-scale protein-ligand structure determination. *Acta Crystallogr D Struct Biol*. 2017; 73 (3) 267–278. [PubMed: 28291762]
- (29). Aimon A, Karageorgis G, Masters J, Dow M, Craven PGE, Ohsten M, Willaume A, Morgentin R, Ruiz-Llamas N, Lemoine H, Kalliokoski T, et al. Realisation of small molecule libraries based on frameworks distantly related to natural products. *Org Biomol Chem*. 2018; 16 (17) 3160–3167. [PubMed: 29645063]
- (30). Foley DJ, Craven PGE, Collins PM, Doveston RG, Aimon A, Talon R, Churcher I, von Delft F, Marsden SP, Nelson A. Synthesis and Demonstration of the Biological Relevance of sp(3)-rich Scaffolds Distantly Related to Natural Product Frameworks. *Chem Eur J*. 2017; 23 (60) 15227–15232. [PubMed: 28983993]
- (31). Jones LH, Summerhill NW, Swain NA, Mills JE. Aromatic chloride to nitrile transformation: medicinal and synthetic chemistry. *Med Chem Comm*. 2010; 1 (5) 309–318.
- (32). Meanwell NA. Fluorine and Fluorinated Motifs in the Design and Application of Bioisosteres for Drug Design. *J Med Chem*. 2018; 61 (14) 5822–5880. [PubMed: 29400967]
- (33). Gillis EP, Eastman KJ, Hill MJ, Donnelly DJ, Meanwell NA. Applications of Fluorine in Medicinal Chemistry. *J Med Chem*. 2015; 58 (21) 8315–8359. [PubMed: 26200936]
- (34). Li W, Yazidi A, Pandya AN, Hegde P, Tong W, Calado Nogueira de Moura V, North EJ, Sygusch J, Jackson M. Mmpl3 as a Target for the Treatment of Drug Resistant Nontuberculosis Mycobacterial Infections. *Front Microbiol*. 2018; 9: 1547. [PubMed: 30042757]
- (35). Williamson DS, Smith GP, Acheson-Dossang P, Bedford ST, Chell V, Chen IJ, Daechsel JCA, Daniels Z, David L, Dokurno P, Hentzer M, et al. Design of Leucine-Rich Repeat Kinase 2 (LRRK2) Inhibitors Using a Crystallographic Surrogate Derived from Checkpoint Kinase 1 (CHK1). *J Med Chem*. 2017; 60 (21) 8945–8962. [PubMed: 29023112]
- (36). Katz JD, Jewell JP, Guerin DJ, Lim J, Dinsmore CJ, Deshmukh SV, Pan B-S, Marshall CG, Lu W, Altman MD, Dahlberg WK, et al. Discovery of a 5Hbenzo[4,5]cyclohepta[1,2-b]pyridin-5-one (MK-2461) Inhibitor of c-Met Kinase for the Treatment of Cancer. *J Med Chem*. 2011; 54 (12) 4092–4108. [PubMed: 21608528]
- (37). Westaway SM, Preston AGS, Barker MD, Brown F, Brown JA, Campbell M, Chung C-W, Drewes G, Eagle R, Garton N, Gordon L, et al. Cell Penetrant Inhibitors of the KDM4 and KDM5 Families of Histone Lysine Demethylases. 2. Pyrido[3,4-d]pyrimidin-4(3H)-one Derivatives. *J Med Chem*. 2016; 59 (4) 1370–1387. [PubMed: 26771203]
- (38). Trabanco AA, Tresadern G, Macdonald GJ, Vega JA, de Lucas AI, Matesanz E, García A, Linares ML, Alonso de Diego SA, Alonso JM, Oehlrich D, et al. Imidazo[1,2-a]pyridines: Orally Active Positive Allosteric Modulators of the Metabotropic Glutamate 2 Receptor. *J Med Chem*. 2012; 55 (6) 2688–2701. [PubMed: 22352782]

- (39). Herr RJ, Cioffi CL, Berlin ML. Convenient Palladium-Catalyzed Preparation of Primary Anilines Using a Fluorous Benzophenone Imine Reagent. *Synlett*. 2004; 5: 0841–0845.
- (40). Vonrhein C, Flensburg C, Keller P, Sharff A, Smart O, Paciorek W, Womack T, Bricogne T. Data processing and analysis with the AutoPROC toolbox. *Acta crystallographica Section D, Biological crystallography*. 2011; 67 (4) 293–302. [PubMed: 21460447]
- (41). Kabsch W. XDS. *Acta crystallographica Section D, Biological crystallography*. 2010; 66 (2) 125–132. [PubMed: 20124692]
- (42). Evans PR. An introduction to data reduction: space-group determination, scaling and intensity statistics. *Acta crystallographica Section D, Biological crystallography*. 2011; 67 (4) 282–292. [PubMed: 21460446]
- (43). Evans PR, Murshudov GN. How good are my data and what is the resolution? *Acta crystallographica Section D, Biological crystallography*. 2013; 69 (7) 1204–1214.
- (44). French SWK, Wilson K. On the treatment of negative intensity observations. *Acta Crystallogr*. 1978; A34: 517–525.
- (45). Winn MD, Ballard CC, Cowtan KD, Dodson EJ, Emsley P, Evans PR, Keegan RM, Krissinel EB, Leslie AG, McCoy A, McNicholas SJ, et al. Overview of the CCP4 suite and current developments. *Acta crystallographica Section D, Biological crystallography*. 2011; 67 (4) 235–242. [PubMed: 21460441]
- (46). McCoy AJ, Grosse-Kunstleve RW, Adams PD, Winn MD, Storoni LC, Read RJ. Phaser Crystallographic Software. *J Appl Crystallogr*. 2007; 40 (4) 658–674. [PubMed: 19461840]
- (47). Murshudov GN, Skubak P, Lebedev AA, Pannu NS, Steiner RA, Nicholls RA, Winn MD, Long F, Vagin AA. REFMAC5 for the refinement of macromolecular crystal structures. *Acta crystallographica Section D, Biological crystallography*. 2011; 67 (4) 355–367. [PubMed: 21460454]
- (48). Adams PD, Afonine PV, Bunkoczi G, Chen VB, Davis IW, Echols N, Headd JJ, Hung LW, Kapral GJ, Grosse-Kunstleve RW, McCoy AJ, et al. PHENIX: a comprehensive Python-based system for macromolecular structure solution. *Acta crystallographica Section D, Biological crystallography*. 2010; 66 (2) 213–221. [PubMed: 20124702]
- (49). Emsley P, Cowtan K. Coot: model-building tools for molecular graphics. *Acta crystallographica Section D, Biological crystallography*. 2004; 60 (12) 2126–2132. [PubMed: 15572765]
- (50). Hodel A, Kim S-H, Brünger AT. Model Bias in Macromolecular Crystal Structures. *Acta Cryst A*. 1992; 48: 851–858.

**Figure 1.**

(a) Schematic representation showing recombination of the allelic exchange substrate (AES) into the chromosome of *M. abscessus subsp. massiliense* followed by replacement of the *purC* gene with a Str cassette and PCR analysis of *M. abscessus subsp. massiliense purC* KO and wt confirming the insertion of the cassette. (b) Essentiality of the *purC* gene: Growth of *M. abscessus subsp. massiliense purC* KO strains on 7H11 ADC plates with or without added hypoxanthine (20 mg/mL).

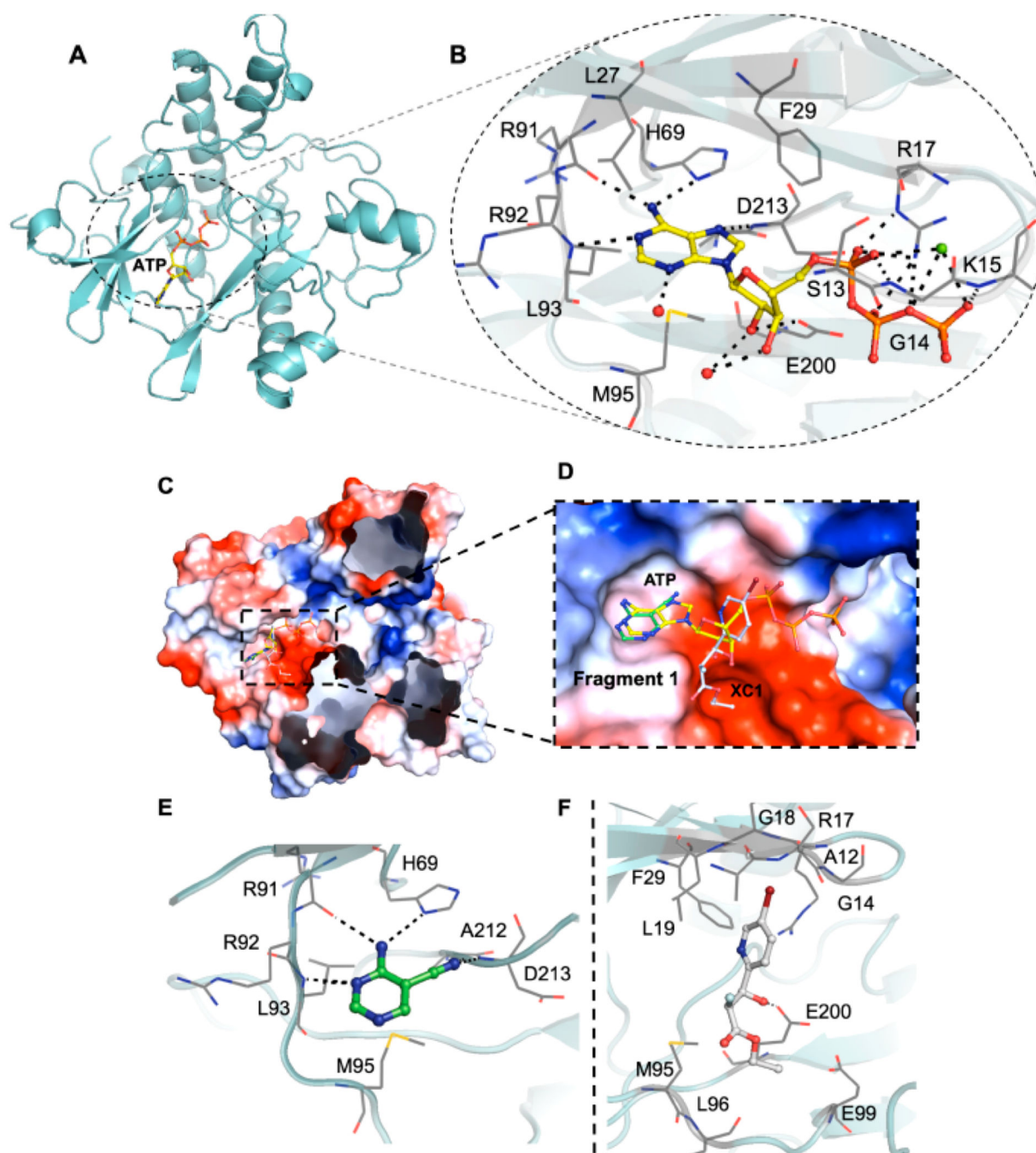
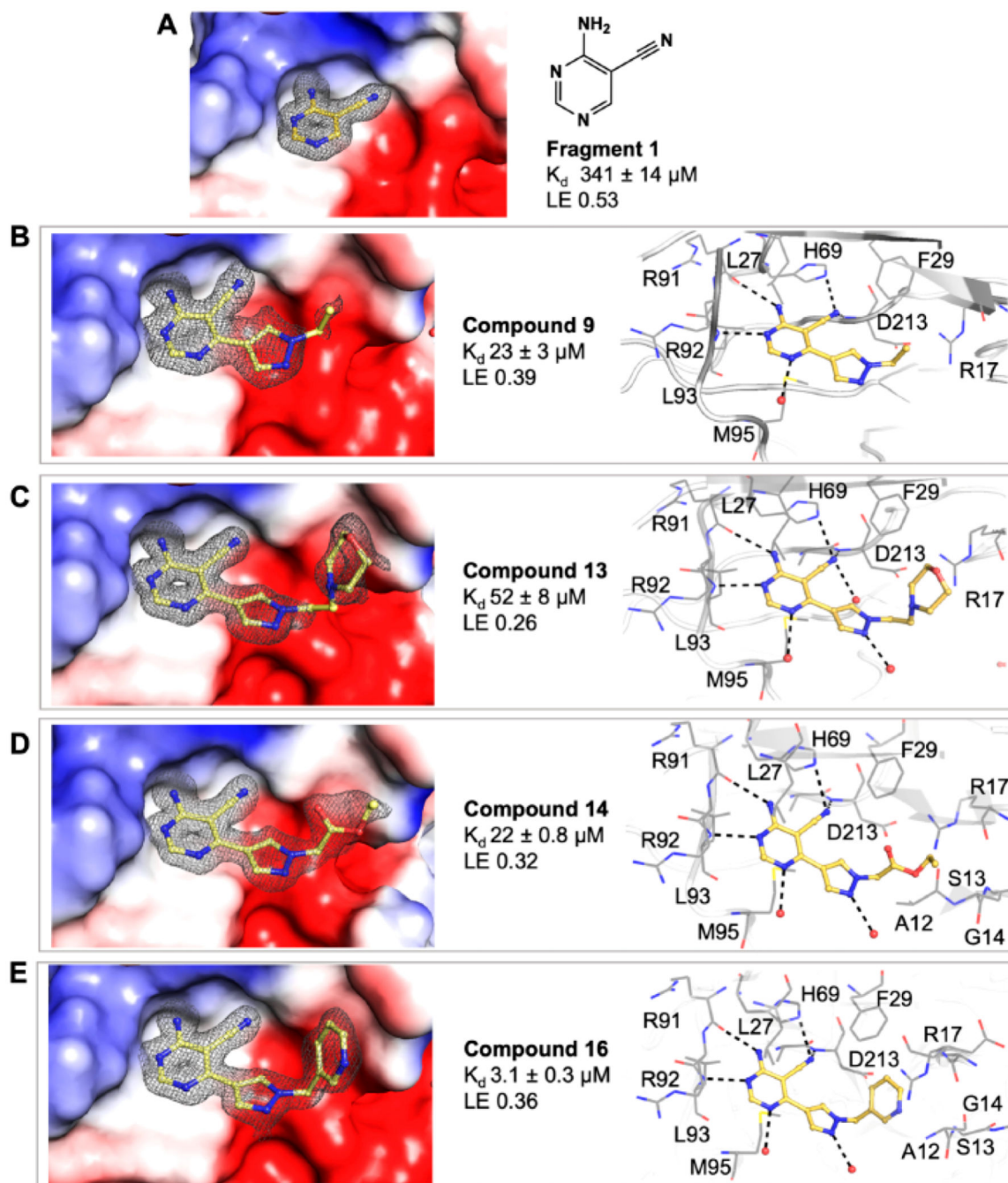


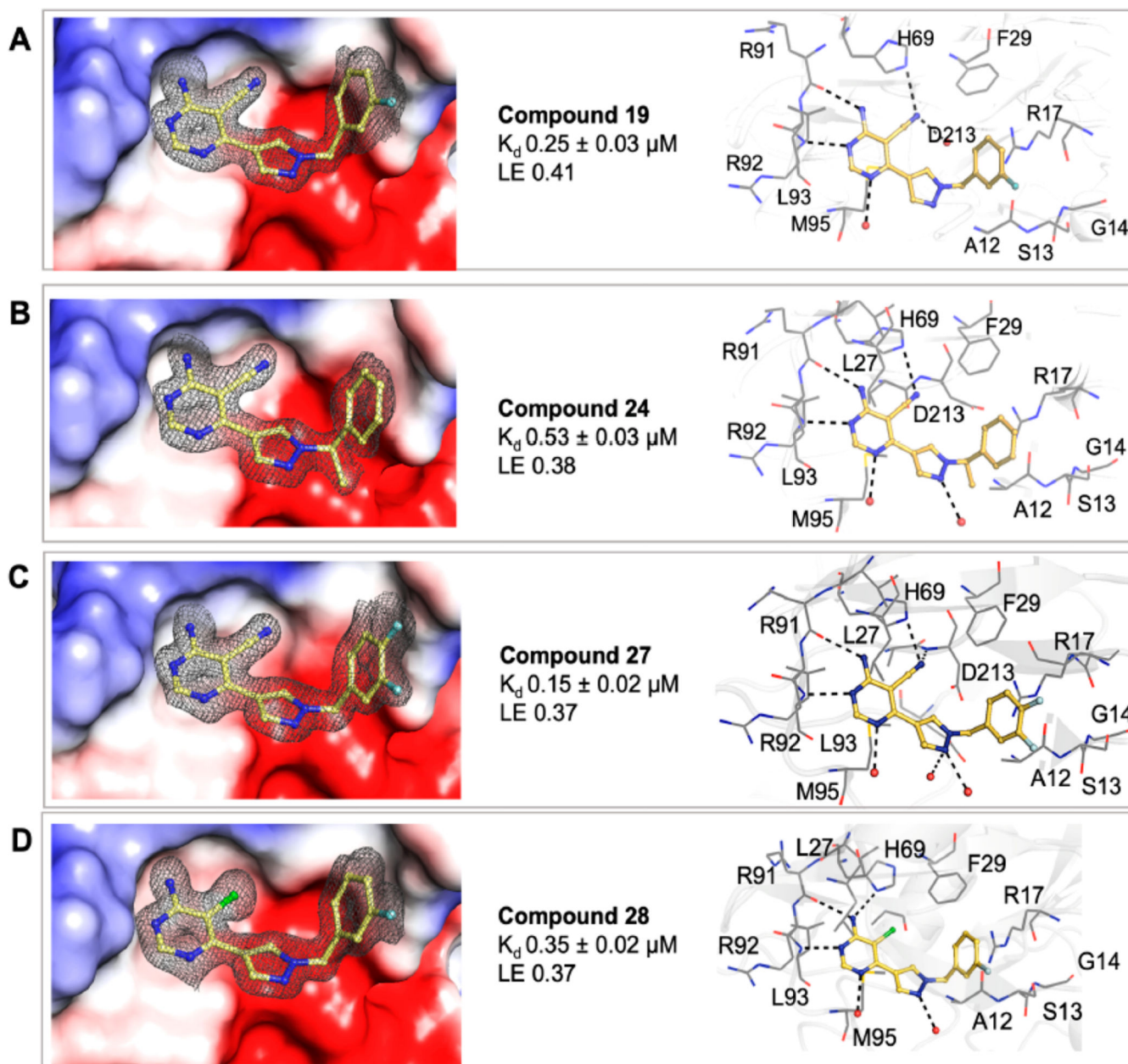
Figure 2.

(a and b) X-ray crystal structure of *Mab* PurC in complex with ATP (PDB code 6YX3). ATP is shown as a yellow stick model with the side chain and key interactions within the active sites highlighted, water molecules as red and Mg^{2+} as green spheres, respectively. (c and d) Overlay of fragment 1 (PDB code 6Z0R) and fragment 2 (PDB code 6Z0Q) in ATP bound PurC. (e) Interactions of fragment 1, shown as a green stick model, with PurC. (f) Interactions of fragment 2, shown as a gray stick model, with PurC. The amino acids are represented as a gray line model.

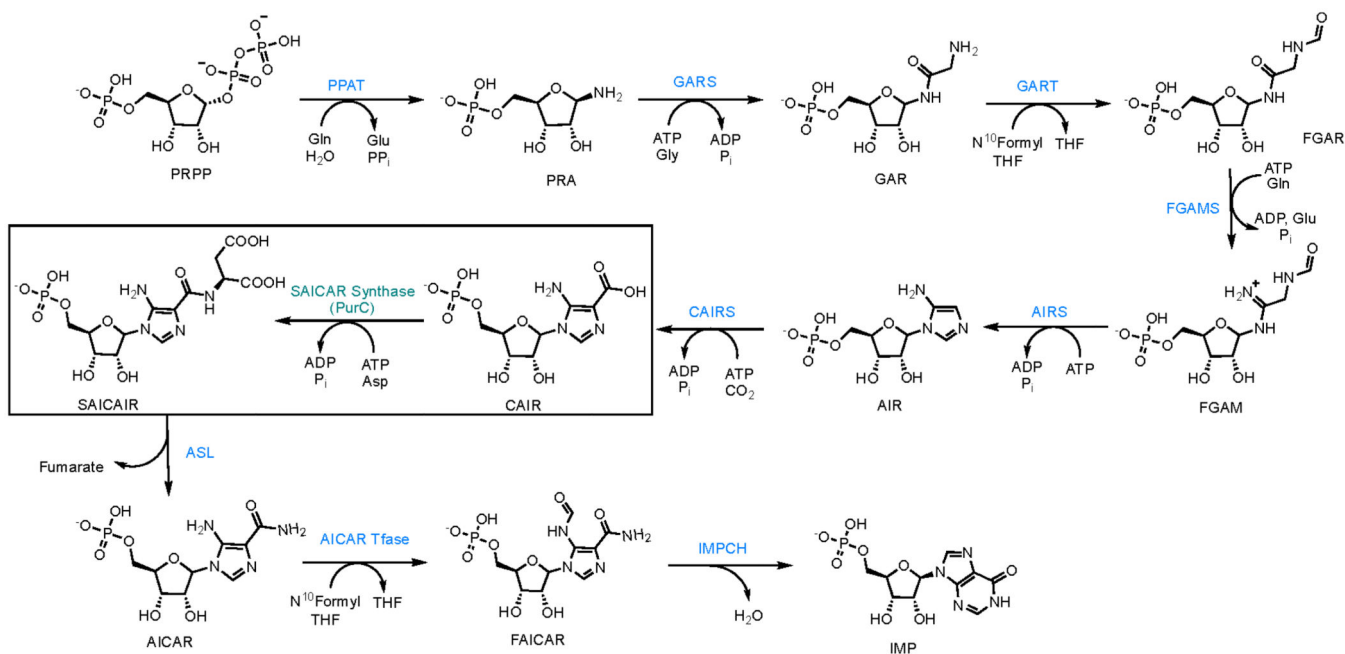
**Figure 3.**

(a) Surface electrostatic representation of the X-ray crystal structures of Mab PurC in complex with fragment **1** (PDB code 6Z0R), occupying the ATP adenine pocket. (b–e) *Mab* PurC in complex with compounds **9** (PDB code 6YY6), **13** (PDB code 6YY8), **14** (PDB code 6YY7), and **16** (PDB code 6YY9) with the corresponding side chain and key interactions within the active sites illustrated beside each figure. The ligands are shown as a yellow stick model with the respective electron density map ($|F_o| - |F_c|$ omit map)

contoured at 2.0σ presented in gray mesh. The interacting amino acids are shown in gray line representation.

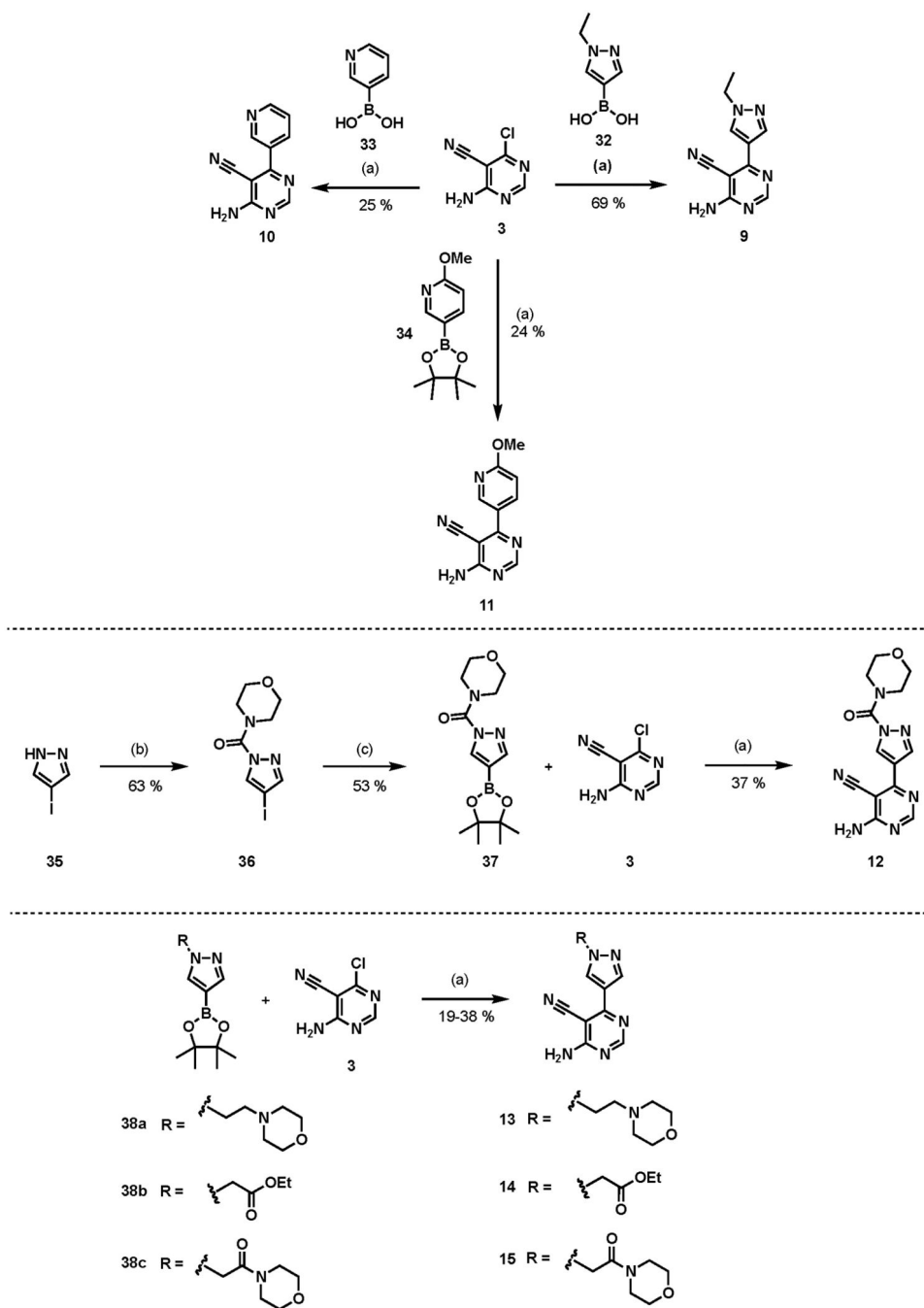
**Figure 4.**

Surface electrostatic representation of the X-ray crystal structures of *Mab* PurC in complex with (a) compound **19** (PDB code 6YYA), (b) compound **24** (PDB code 6YYB), (c) compound **27** (PDB code 6YYD), and (d) compound **28** (PDB code 6YYC) with the side chain and key interactions within the active sites illustrated beside each figure. The ligands are shown as a yellow stick model with the respective electron density map ($|F_o| - |F_c|$ omit map) contoured at 2.0σ presented in gray mesh. The interacting amino acids are shown in a gray line representation.



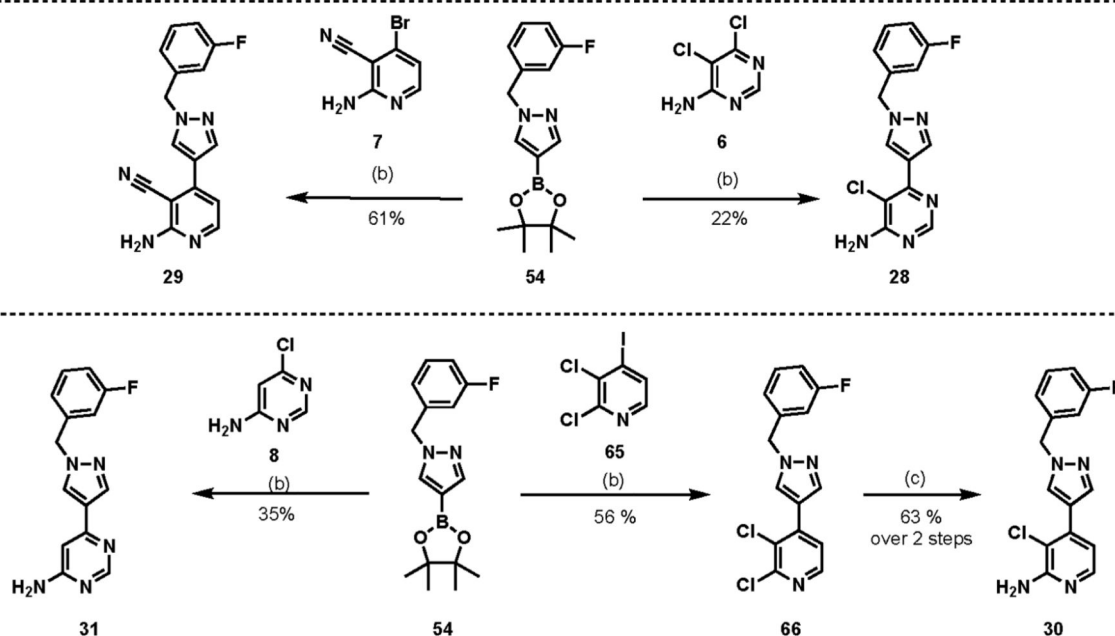
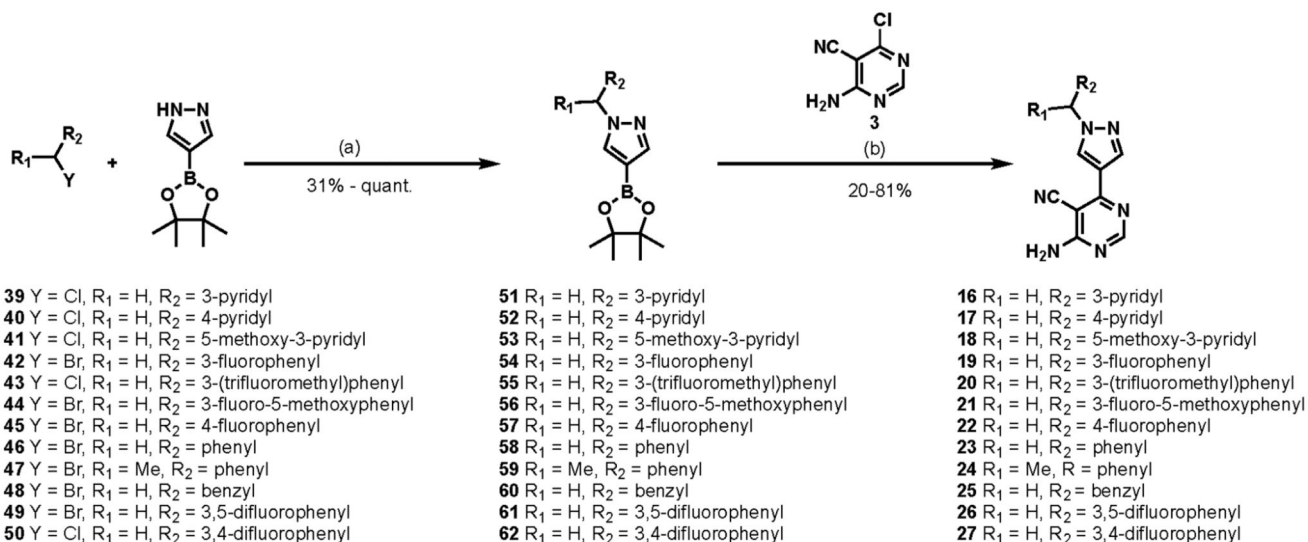
Scheme 1. Purine Biosynthetic Pathway, the Pathway Transforms PRPP (Phosphoribosyl Pyrophosphate) into IMP (Inosine Monophosphate) in 10 Biosynthetic Steps^a

^aSAICAR synthetase (PurC) catalyzes seventh step in the biosynthetic pathway which transforms CAIR (carboxyaminoimidazole ribonucleotide) into SAICAIR (succinylaminoimidazole carboxamide ribonucleotide) using ATP and L-aspartate.



Scheme 2. Synthesis of 4-Aminopyrimidine and 2-Aminopyridine Derivatives^a

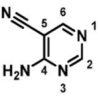
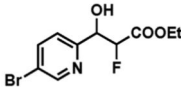
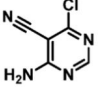
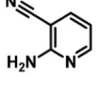
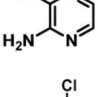
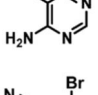
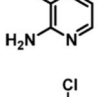
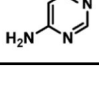
^aReagents and conditions: (a) Pd(*t*-Bu₃P)₂, KF, 1,4-dioxane, water, MW irradiation, 150 °C, 40 min; (b) 4-morpholinecarbonyl chloride, Et₃N, DCM, overnight; (c) B₂pin₂, Pd(dppf)Cl₂.DCM, KOAc, DMSO, MW irradiation, 80 °C, 3 h.



Scheme 3. Synthesis of 4-Aminopyrimidine and 2-Aminopyridine Derivatives^a

^aReagents and conditions: (a) K₂CO₃ or Cs₂CO₃, MeCN, overnight. (b) Pd(*t*-Bu₃P)₂, KF, 1,4-dioxane, water, MW irradiation, 150 °C, 40 min. (c) (i) Pd₂(dba)₃, BINAP, *t*-BuONa, benzophenone imine, toluene, 80 °C, overnight; (ii) 1 M HCl, THF, 5 h.

Table 1
Biophysical Data for Selected Fragments Showing the Change in Protein Melting
Temperatures (T_m), Binding Affinities (K_d), and Ligand Efficiencies (LE)^a

Compound	Chemical structure	T_m (°C) ^b	MabPurC K_d (μM)	LE ^d
1		+3.6	341 ± 14	0.53
2		ND	ND	–
3		+4.0	159 ± 9	0.52
4		+1.7 ^c	1060 ± 252	0.45
5		+1.0	971 ± 29	0.51
6		+2.5	442 ± 22	0.51
7		+1.7	ND	–
8		+0.7	ND	–

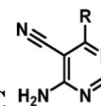
^aND not determined.

^b5 mM ligand and 100 μM MabPurC.

^c3 mM ligand and 70 μM MabPurC.

^dkcal mol⁻¹ per heavy atom.

Table 2

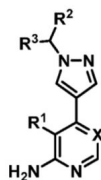
Exploration of SAR on the 6-Position of the Pyrimidine Ring against *MabPurC*

Compound	R	T _m (°C) ^a	<i>MabPurC</i> K _d (μM)	LE ^b
1	H	+1.1	341 ± 14	0.53
3	Cl	+2.1	159 ± 9	0.52
9		+4.4	23 ± 3	0.39
10		+2.0	588 ± 26	0.28
11		+2.6	84 ± 10	0.33

^a 1 mM ligand and 100 μM *MabPurC*.

^b kcal mol⁻¹ per heavy atom.

Table 3
Biophysical Data of 4-Amino-6-(pyrazol-4-yl)pyrimidine Derivatives against *MabPurC*^a



Compound	R ¹	R ²	R ³	X	T _m (°C) ^b	<i>MabPurC</i> K _d (μM)	LE ^d
9	CN	Me	H	N	+4.4	23 ± 3	0.39
12	CN		=o	N	+2.9	45 ± 5	0.27
13	CN		H	N	+3.5	52 ± 8	0.26
14	CN		H	N	+4.5	22 ± 0.8	0.32
15	CN		H	N	+2.6	47 ± 6	0.26
16	CN	3-pyridyl	H	N	+6.2	3.1 ± 0.3	0.36
17	CN	4-pyridyl	H	N	+6.0	7.5 ± 0.5	0.33
18	CN	5-methoxy-3-pyridyl	H	N	+6.5	2.1 ± 0.2	0.34
19	CN	3-fluorophenyl	H	N	+8.3	0.25 ± 0.03	0.41
20	CN	3-(trifluoromethyl)phenyl	H	N	+5.3	ND	-
21	CN	3-fluoro-5-methoxyphenyl	H	N	+8.8 ^a	ND ^e	-
22	CN	4-fluorophenyl	H	N	+9.4	0.22 ± 0.02	0.41
23	CN	phenyl	H	N	+9.3	0.28 ± 0.03	0.43
24	CN	phenyl	Me	N	+7.5	0.53 ± 0.03	0.38
25	CN	benzyl	H	N	+5.3	ND	-
26	CN	3,5-difluorophenyl	H	N	+8.7 ^e	0.24 ± 0.05	0.37
27	CN	3,4-difluorophenyl	H	N	+9.0	0.15 ± 0.02	0.37
28	Cl	3-fluorophenyl	H	N	+7.1	0.35 ± 0.02	0.39
29	CN	3-fluorophenyl	H	CH	+5.1	1.4 ± 0.06	0.36
30	Cl	3-fluorophenyl	H	CH	+2.6 ^c	ND	-
31	H	3-fluorophenyl	H	N	+4.1	ND	-

^aND not determined.

^b1 mM ligand and 100 μM *MabPurC*

^c0.5 mM ligand and 100 μM *MabPurC*

^dkcal mol⁻¹ per heavy atom.

^eDue to poor solubility.

Table 4
Antimycobacterial Profile of 4-Amino-6-(pyrazol-4-yl)pyrimidine Derivatives Screened against *Mab* and *Mtb*

compound	<i>Mab</i> PurC K_d (μ M)	$\log P^a$	<i>Mab</i> MIC (μ M) ^b	<i>Mtb</i> MIC (μ M) ^c
amikacin	NA	-8.9	3.1	12.5
12	45 ± 5	-0.8	50–200	NA
13	52 ± 8	-0.6	50–200	NA
14	22 ± 0.8	-0.4	50–200	NA
15	47 ± 6	-1.6	200–400	50
16	3.1 ± 0.3	0.2	50–200	50
17	7.5 ± 0.5	0.2	50–200	50
18	2.1 ± 0.2	0.03	50–200	50
19	0.25 ± 0.03	1.6	50–200	50
22	0.22 ± 0.02	1.6	50–200	50
23	0.28 ± 0.03	1.5	50–200	50
24	0.53 ± 0.03	1.8	50–200	50
26	0.24 ± 0.05	1.8	50–200	50
27	0.15 ± 0.02	1.8	50–200	50
28	0.35 ± 0.02	2.2	50–200	25
29	1.4 ± 0.06	1.8	50–200	25

^a $\log P$ was calculated using ChemDraw Professional Version 20.0

^b *Mycobacterium abscessus subspecies abscessus* (ATCC 19977) transformed with pmv310 plasmid expressing Lux ABDCE operon, grown in Middlebrook 7H9 broth supplemented with ADC.

^c *Mycobacterium tuberculosis* leuD panCD (Bleupan) transformed with pSMT1 expressing Lux AB and GFP, grown in Middlebrook 7H9 broth supplemented with 0.5% glycerol, 0.05% Tween 80 (removed for 24 h prior to experiments), 10% OADC (BD), 0.05 mg/mL L-leucine, and 0.024 mg/mL calcium pantothenate, hygromycin, and zeocin (removed for 24 h prior to experiments).